Umeda and Ozaki *Earth, Planets and Space* (2023) 75:157
https://doi.org/10.1186/s40623-023-01902-8

Earth, Planets and Space

TECHNICAL REPORT

Open Access

Advanced numerical techniques for time integration of relativistic equations of motion for charged particles

Takayuki Umeda[1*] and Riku Ozaki[1]

Abstract

Advanced numerical techniques for solving the relativistic equations of motion for charged particles are provided. A new fourth-order integrator is developed by combining the Taylor series expansion of the numerical angle of relativistic gyration and the fourth-order Runge–Kutta method for integrating the Lorentz factor. The new integrator gives the exact relativistic E-cross-B drift velocity, but has a numerical accuracy much higher than the classic fourth-order Runge–Kutta integrator.

Keywords Equations of motion, Charged particle, Relativity, Higher-order integration, Taylor expansion, Runge–Kutta method

Graphical Abstract

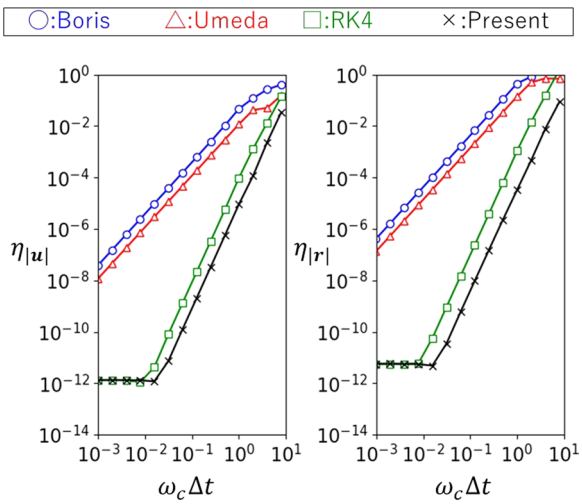

*Correspondence:
Takayuki Umeda
umeda@isee.nagoya-u.ac.jp
Full list of author information is available at the end of the article

Background

The relativistic equations of motion for charged particles are important for planetary and space science studies, especially for relativistic particle accelerations at collisionless shocks (Umeda and Yamazaki 2006; Nakanotani et al. 2018) and in planetary radiation belts (Katoh 2014; Katoh and Omura 2016; Hiraga and Omura 2020; Omura 2021; Fujiwara et al. 2022). The classic fourth-order Runge–Kutta integrator (RK4) (Runge 1895; Kutta 1901) has been used over many years for solving the relativistic equations of motion for charged particles. Although RK4 has a high numerical accuracy, it does not satisfy any of conservation laws.

As an alternative to RK4, the Boris integrator (Boris 1970) has been used over fifty years in particle-in-cell simulations. The Boris integrator has the second-order accuracy in time. The Boris integrator conserves the kinetic energy during the gyration of charged particles in a magnetic field. This property makes the phase-space trajectories of particles with the Boris integrator more accurate than with the classic RK4 in a long-term time integration (Qin et al. 2013; He et al. 2015). The Boris integrator also provides the exact *non-relativistic* $E \times B$ drift velocity. It has been known, however, that the Boris integrator has a numerical error in the gyration angle per time step.

It is also known that the Boris integrator has a large numerical error in the drift velocity of the *relativistic* $E \times B$ drift (Vay 2008; Zhang et al. 2015; Higuera and Cary 2017; Ripperda et al. 2018). There have been several attempts for obtaining a more accurate relativistic $E \times B$ drift velocity, such as the Vay integrator (Vay 2008) and the Higuera–Cary integrator (Higuera and Cary 2017). These explicit integrators reduce numerical errors in the phase-space trajectories of particles when a particle velocity vector is close to the guiding-center velocity vector only. For a velocity vector far from the guiding-center velocity vector, a numerical error in the phase-space trajectories of particles with the Boris integrator is smaller than that with the Vay or the Higuera–Cary integrators.

Based on the analytic solution to the relativistic $E \times B$ drift motion, a new explicit integrator for the relativistic equations of motion for a charged particle has been developed recently (Umeda 2023). The new integrator (hereafter the Umeda integrator) has the second-order accuracy in time and provides the exact relativistic $E \times B$ drift velocity. However, the Umeda integrator has a numerical error in the gyration angle per time step as the Boris integrator. A purpose of the present study is to increase the numerical accuracy of the Umeda integrator.

Brief introduction to the Umeda integrator

Let us start with the relativistic equations of motion for a charged particle with a position vector $\boldsymbol{r}$, a velocity vector $\boldsymbol{v}$, a mass m, and a charge q, which expresses the acceleration of charged particles by electric field $\boldsymbol{E}$ and magnetic field $\boldsymbol{B}$:

$$\frac{\mathrm{d}\boldsymbol{r}}{\mathrm{d}t} = \boldsymbol{v}, \tag{1a}$$

$$\frac{\mathrm{d}}{\mathrm{d}t}(\gamma \boldsymbol{v}) = \frac{q}{m}(\boldsymbol{E} + \boldsymbol{v} \times \boldsymbol{B}), \tag{1b}$$

where γ is the relativistic Lorentz factor given as:

$$\gamma = \frac{c}{\sqrt{c^2 - |\boldsymbol{v}|^2}}, \tag{2}$$

with c being the speed of light.

To simplify Eq.(1b), a motion of a charged particle is separated into motions in the directions parallel and perpendicular to a magnetic field. The velocity components parallel and perpendicular to a magnetic field are given as follows:

$$\boldsymbol{v}_\parallel = \frac{(\boldsymbol{v} \cdot \boldsymbol{B})\boldsymbol{B}}{|\boldsymbol{B}|^2}, \tag{3a}$$

$$\boldsymbol{v}_\perp = \boldsymbol{v} - \boldsymbol{v}_\parallel = -\frac{(\boldsymbol{v} \times \boldsymbol{B}) \times \boldsymbol{B}}{|\boldsymbol{B}|^2}. \tag{3b}$$

Then, Eq.(1b) is separated into two components parallel and perpendicular to the magnetic field as follows:

$$\frac{\mathrm{d}\boldsymbol{u}_\parallel}{\mathrm{d}t} = \frac{q}{m}\boldsymbol{E}_\parallel, \tag{4a}$$

$$\begin{aligned}\frac{\mathrm{d}\boldsymbol{u}_\perp}{\mathrm{d}t} &= \frac{q}{m}(\boldsymbol{v} \times \boldsymbol{B}) + \frac{q}{m}\boldsymbol{E}_\perp = \frac{q}{m}\{(\boldsymbol{v} - \boldsymbol{v}_E) \times \boldsymbol{B}\} \\ &= \frac{q}{m}(\boldsymbol{v} \times \boldsymbol{B}) - \frac{q}{m}\left(\frac{\boldsymbol{E} \times \boldsymbol{B}}{|\boldsymbol{B}|^2} \times \boldsymbol{B}\right) \\ &= \frac{q}{m}(\boldsymbol{v} \times \boldsymbol{B}) + \frac{q}{m}\left\{\boldsymbol{E} - \frac{(\boldsymbol{E} \cdot \boldsymbol{B})\boldsymbol{B}}{|\boldsymbol{B}|^2}\right\},\end{aligned} \tag{4b}$$

where $\boldsymbol{u} \equiv \gamma \boldsymbol{v}$ is a momentum vector and $\boldsymbol{v}_E$ is the $E \times B$ drift velocity vector

$$\boldsymbol{v}_E = \frac{\boldsymbol{E} \times \boldsymbol{B}}{|\boldsymbol{B}|^2},$$

with $\boldsymbol{E}_\parallel$ and $\boldsymbol{E}_\perp$ being the electric field components parallel and perpendicular to the magnetic field, respectively,

$$\boldsymbol{E}_{\parallel} = \frac{(\boldsymbol{E}\cdot\boldsymbol{B})\boldsymbol{B}}{|\boldsymbol{B}|^2},$$
$$\boldsymbol{E}_{\perp} = \boldsymbol{E} - \boldsymbol{E}_{\parallel} = -\frac{(\boldsymbol{E}\times\boldsymbol{B})\times\boldsymbol{B}}{|\boldsymbol{B}|^2} = -\boldsymbol{v}_E\times\boldsymbol{B}.$$

Let us take a coordinate system such that $\boldsymbol{B}\parallel z$ and $\boldsymbol{E}\parallel y$ (i.e., $\boldsymbol{E}\times\boldsymbol{B}\parallel x$). For the relativistic $E\times B$ drift (i.e., $c|\boldsymbol{B}|>|\boldsymbol{E}|$) with a constant electromagnetic field, the perpendicular component of the momentum vector in the present coordinate system, i.e., $\boldsymbol{u}_{\perp}=(u_x,u_y)$ moves along the following elliptical trajectory (Friedman and Semon 2005):

$$(u_x-\gamma_B\gamma_E v_E)^2+\gamma_E^2u_y^2=C, \tag{5}$$

where C is a constant, γ_E is the Lorentz factor of the $E\times B$ drift velocity $v_E=E_y/B_z$,

$$\gamma_E\equiv\frac{c}{\sqrt{c^2-v_E^2}},$$

and γ_B is a correction factor due to the gradient-B-type drift caused by $\mathrm{d}\gamma/\mathrm{dt}\neq 0$, which is also known as a "boosted" Lorentz factor (Ripperda et al. 2018):

$$\gamma_B\equiv\frac{c^2-v_Ev_x}{\sqrt{(c^2-v_E^2)(c^2-v_x^2-v_y^2-v_z^2)}}\equiv\gamma_E\left(\gamma-\frac{\boldsymbol{v}_E\cdot\boldsymbol{u}}{c^2}\right). \tag{6}$$

The boosted Lorentz factor is constant on the elliptical trajectory in Eq.(5), which is obtained by taking the time derivative of γ_B as follows:

$$\begin{aligned}\frac{\boldsymbol{v}_E}{c^2}\cdot\frac{\mathrm{d}\boldsymbol{u}}{\mathrm{dt}} &= \frac{\boldsymbol{E}\times\boldsymbol{B}}{c^2|\boldsymbol{B}|^2}\cdot\frac{q}{m}(\boldsymbol{E}+\boldsymbol{v}\times\boldsymbol{B})\\ &= \frac{q}{mc^2|\boldsymbol{B}|^2}(\boldsymbol{E}\times\boldsymbol{B})\cdot(\boldsymbol{v}\times\boldsymbol{B})\\ &= \frac{q}{mc^2}\boldsymbol{E}\cdot\boldsymbol{v}=\frac{\mathrm{d}\gamma}{\mathrm{dt}}.\end{aligned}$$

Here, a similar approach to Zenitani and Umeda (2018) for the Boris integrator is used. The elliptical trajectory in the u_x-u_y space is written by using the elliptical rotation matrix as follows:

$$\begin{pmatrix} u_x^{t+\frac{\Delta t}{2}}-\gamma_B\gamma_E v_E \\ u_y^{t+\frac{\Delta t}{2}}\end{pmatrix} = \begin{pmatrix} \cos\left(\frac{\omega_c\Delta\tau}{\gamma_E}\right) & \gamma_E\sin\left(\frac{\omega_c\Delta\tau}{\gamma_E}\right)\\ -\frac{1}{\gamma_E}\sin\left(\frac{\omega_c\Delta\tau}{\gamma_E}\right) & \cos\left(\frac{\omega_c\Delta\tau}{\gamma_E}\right)\end{pmatrix}\begin{pmatrix} u_x^{t-\frac{\Delta t}{2}}-\gamma_B\gamma_E v_E \\ u_y^{t-\frac{\Delta t}{2}}\end{pmatrix},$$

where $\omega_c\equiv q|\boldsymbol{B}|/m$ is the gyro frequency and τ is the proper time in relativity,

$$\int_{\tau-\frac{\Delta\tau}{2}}^{\tau+\frac{\Delta\tau}{2}}\gamma(\tau')\mathrm{d}\tau'=\left(\mathrm{t}+\frac{\Delta\mathrm{t}}{2}\right)-\left(\mathrm{t}-\frac{\Delta\mathrm{t}}{2}\right)=\Delta\mathrm{t}. \tag{7}$$

This is rewritten by using the half-angle formula of trigonometric functions together with Eq.(6) as follows:

$$\begin{aligned}\begin{pmatrix} u_x^{t+\frac{\Delta t}{2}}\\ u_y^{t+\frac{\Delta t}{2}}\end{pmatrix} = \begin{pmatrix} u_x^{t-\frac{\Delta t}{2}}\\ u_y^{t-\frac{\Delta t}{2}}\end{pmatrix} &- \begin{pmatrix} \frac{2\tan^2\left(\frac{\omega_c\Delta\tau}{2\gamma_E}\right)}{1+\tan^2\left(\frac{\omega_c\Delta\tau}{2\gamma_E}\right)} & -\gamma_E\frac{2\tan\left(\frac{\omega_c\Delta\tau}{2\gamma_E}\right)}{1+\tan^2\left(\frac{\omega_c\Delta\tau}{2\gamma_E}\right)}\\ \gamma_E\frac{2\tan\left(\frac{\omega_c\Delta\tau}{2\gamma_E}\right)}{1+\tan^2\left(\frac{\omega_c\Delta\tau}{2\gamma_E}\right)} & \frac{2\tan^2\left(\frac{\omega_c\Delta\tau}{2\gamma_E}\right)}{1+\tan^2\left(\frac{\omega_c\Delta\tau}{2\gamma_E}\right)}\end{pmatrix}\begin{pmatrix} u_x^{t-\frac{\Delta t}{2}}\\ u_y^{t-\frac{\Delta t}{2}}\end{pmatrix}\\ &+ \begin{pmatrix} \gamma_B\frac{2\tan^2\left(\frac{\omega_c\Delta\tau}{2\gamma_E}\right)}{1+\tan^2\left(\frac{\omega_c\Delta\tau}{2\gamma_E}\right)} & -\gamma^{t-\frac{\Delta t}{2}}\frac{2\tan\left(\frac{\omega_c\Delta\tau}{2\gamma_E}\right)}{1+\tan^2\left(\frac{\omega_c\Delta\tau}{2\gamma_E}\right)}\\ \gamma^{t-\frac{\Delta t}{2}}\frac{2\tan\left(\frac{\omega_c\Delta\tau}{2\gamma_E}\right)}{1+\tan^2\left(\frac{\omega_c\Delta\tau}{2\gamma_E}\right)} & \gamma_B\frac{2\tan^2\left(\frac{\omega_c\Delta\tau}{2\gamma_E}\right)}{1+\tan^2\left(\frac{\omega_c\Delta\tau}{2\gamma_E}\right)}\end{pmatrix}\begin{pmatrix}\gamma_E v_E\\ 0\end{pmatrix}.\end{aligned} \tag{8}$$

The gyration angle per proper time step $\Delta\tau$ is approximated as:

$$\tan\left(\frac{\omega_c\Delta\tau}{2\gamma_E}\right)\approx\frac{q\Delta\tau}{2m\gamma_E}|\boldsymbol{B}|.$$

Equation (8) is then rewritten in the following vector form:

$$\begin{aligned}\boldsymbol{u}_\perp^{t+\frac{\Delta t}{2}}=&\boldsymbol{u}_\perp^{t-\frac{\Delta t}{2}}-2\beta_U\left(\frac{q\Delta\tau}{2m\gamma_E}|\boldsymbol{B}|\right)^2\boldsymbol{u}_\perp^{t-\frac{\Delta t}{2}}+\beta_U\frac{q\Delta\tau}{m}\left(\boldsymbol{u}^{t-\frac{\Delta t}{2}}\times\boldsymbol{B}\right)\\&+2\beta_U\frac{\gamma_B}{\gamma_E}\left(\frac{q\Delta\tau}{2m}|\boldsymbol{B}|\right)^2\boldsymbol{v}_E-\beta_U\gamma^{t-\frac{\Delta t}{2}}\frac{q\Delta\tau}{m}(\boldsymbol{v}_E\times\boldsymbol{B}),\end{aligned}\tag{9}$$

where

$$\beta_U=\frac{1}{1+\left(\frac{q\Delta\tau}{2m\gamma_E}|\boldsymbol{B}|\right)^2}.$$

The time-development equation for the momentum vector $\boldsymbol{u}$ is obtained by adding the momentum component parallel to the ambient magnetic field $\boldsymbol{u}_\parallel$ to Eq.(9):

$$\begin{aligned}\boldsymbol{u}^{t+\frac{\Delta t}{2}}=&\boldsymbol{u}^{t-\frac{\Delta t}{2}}+\frac{q\Delta t}{m}\boldsymbol{E}+\beta_U\frac{q\Delta\tau}{m}\left(\boldsymbol{u}^{t-\frac{\Delta t}{2}}\times\boldsymbol{B}\right)+2\beta_U\left(\frac{q\Delta\tau}{2m\gamma_E}\right)^2\\&\left\{\left(\boldsymbol{u}^{t-\frac{\Delta t}{2}}\times\boldsymbol{B}\right)\times\boldsymbol{B}\right\}\quad+2\beta_U\frac{\gamma_B}{\gamma_E}\left(\frac{q\Delta\tau}{2m}|\boldsymbol{B}|\right)^2\boldsymbol{v}_E\\&+\left(\frac{q\Delta t}{m}-\beta_U\gamma^{t-\frac{\Delta t}{2}}\frac{q\Delta\tau}{m}\right)(\boldsymbol{v}_E\times\boldsymbol{B}).\end{aligned}\tag{10}$$

The proper time step is approximated by:

$$\int_{\tau-\frac{\Delta\tau}{2}}^{\tau+\frac{\Delta\tau}{2}}\gamma(\tau')\mathrm{d}\tau'\approx\Gamma\Delta\tau=\Delta\mathrm{t}.\tag{11}$$

The previous study (Umeda 2023) chose

$$\Gamma=\gamma_-\equiv\frac{\sqrt{c^2+\left|\boldsymbol{u}^{t-\frac{\Delta t}{2}}+\frac{q\Delta t}{2m}\boldsymbol{E}\right|^2}}{c},$$

which has been used in the Boris integrator (Boris 1970).

Note that the Boris integrator (Boris 1970) is also rewritten with the same form as Eq.(10):

$$\begin{aligned}\boldsymbol{u}^{t+\frac{\Delta t}{2}}=&\boldsymbol{u}^{t-\frac{\Delta t}{2}}+\frac{q\Delta t}{m}\boldsymbol{E}+\beta_B\frac{q\Delta t}{m\gamma_-}\left(\boldsymbol{u}^{t-\frac{\Delta t}{2}}\times\boldsymbol{B}\right)+2\beta_B\left(\frac{q\Delta t}{2m\gamma_-}\right)^2\\&\left\{\left(\boldsymbol{u}^{t-\frac{\Delta t}{2}}\times\boldsymbol{B}\right)\times\boldsymbol{B}\right\}\\&+2\beta_B\gamma_-\left(\frac{q\Delta t}{2m\gamma_-}|\boldsymbol{B}|\right)^2\boldsymbol{v}_E+\frac{q\Delta t}{m}(1-\beta_B)(\boldsymbol{v}_E\times\boldsymbol{B}),\end{aligned}\tag{12}$$

where

$$\beta_B=\frac{1}{1+\left(\frac{q\Delta t}{2m\gamma_-}|\boldsymbol{B}|\right)^2}.$$

The Umeda integrator (Umeda 2023) corresponds to the Boris integrator (Boris 1970) if $\boldsymbol{E}=0$. The Umeda integrator also approaches to the non-relativistic Boris integrator as $c\to\infty$ (i.e., $\gamma\to1$).

Construction of higher-order integrator

For an arbitrary time step Δt, the momentum vector $\boldsymbol{u}$ obtained with the Umeda integrator (Umeda 2023) is always on the elliptical trajectory, which is the analytic solution to the relativistic $E\times B$ drift in a uniform and constant electromagnetic field. That is, the Umeda integrator satisfies $\mathrm{d}\gamma_\mathrm{B}/\mathrm{dt}=0$ and gives the exact relativistic $E\times B$ drift velocity. However, a numerical error in the gyration angle becomes larger as the time step Δt becomes larger. Below, numerical techniques for reducing numerical errors are given.

Taylor series expansion of tangent function

The Taylor series expansion of the tangent function in Eq.(8) with Eq.(11) is given as follows (Kato and Zenitani 2021):

$$\begin{aligned}&\tan\left(\frac{q\Delta\tau}{2m\gamma_E}|\boldsymbol{B}|\right)\\&\approx\frac{q\Delta t}{2m\gamma_E\Gamma}|\boldsymbol{B}|\left\{1+\frac{1}{3}\left(\frac{q\Delta t}{2m\gamma_E\Gamma}|\boldsymbol{B}|\right)^2\right.\\&\left.+\frac{2}{15}\left(\frac{q\Delta t}{2m\gamma_E\Gamma}|\boldsymbol{B}|\right)^4+\cdots\right\}.\end{aligned}\tag{13}$$

The Boris integrator (Boris 1970) and the previous study (Umeda 2023) used the first (i.e., Δt) term only. The time-development equation for the momentum vector $\boldsymbol{u}$ is written in the following form by using Eq.(13):

$$\boldsymbol{u}^{t+\frac{\Delta t}{2}}=\boldsymbol{u}^{t-\frac{\Delta t}{2}}+\mathcal{F}\left(\frac{1}{\Gamma},\Delta t\right),\tag{14a}$$

$$\begin{aligned}\mathcal{F}\left(\frac{1}{\Gamma},\Delta t\right)\equiv&\frac{q\Delta t}{m}\boldsymbol{E}+f_1\left(\boldsymbol{u}^{t-\frac{\Delta t}{2}}\times\boldsymbol{B}\right)+f_2\left\{\left(\boldsymbol{u}^{t-\frac{\Delta t}{2}}\times\boldsymbol{B}\right)\times\boldsymbol{B}\right\}\\&+f_3\boldsymbol{v}_E+f_4(\boldsymbol{v}_E\times\boldsymbol{B}),\end{aligned}\tag{14b}$$

$$\begin{aligned}f_1=\frac{\gamma_E}{|\boldsymbol{B}|}\sin\left(\frac{q\Delta t}{m\gamma_E\Gamma}|\boldsymbol{B}|\right)&=2\beta_U\frac{\gamma_E}{|\boldsymbol{B}|}\tan\left(\frac{q\Delta t}{2m\gamma_E\Gamma}|\boldsymbol{B}|\right)\\&\approx\beta_U\frac{q\Delta t}{m\Gamma}\left\{1+\frac{1}{3}\left(\frac{q\Delta t}{2m\gamma_E\Gamma}|\boldsymbol{B}|\right)^2+\frac{2}{15}\left(\frac{q\Delta t}{2m\gamma_E\Gamma}|\boldsymbol{B}|\right)^4+\cdots\right\},\end{aligned}\tag{14c}$$

$$f_2 = \frac{1}{|\boldsymbol{B}|^2}\left\{1-\cos\left(\frac{q\Delta t}{m\gamma_E\Gamma}|\boldsymbol{B}|\right)\right\} = 2\beta_U\frac{1}{|\boldsymbol{B}|^2}\tan^2\left(\frac{q\Delta t}{2m\gamma_E\Gamma}|\boldsymbol{B}|\right)$$
$$\approx 2\beta_U\left(\frac{q\Delta t}{2m\gamma_E\Gamma}\right)^2\left\{1+\frac{1}{3}\left(\frac{q\Delta t}{2m\gamma_E\Gamma}|\boldsymbol{B}|\right)^2+\frac{2}{15}\left(\frac{q\Delta t}{2m\gamma_E\Gamma}|\boldsymbol{B}|\right)^4+\cdots\right\}^2, \tag{14d}$$

$$f_3 = \gamma_B\gamma_E\left\{1-\cos\left(\frac{q\Delta t}{m\gamma_E\Gamma}|\boldsymbol{B}|\right)\right\} = 2\beta_U\gamma_B\gamma_E\tan^2\left(\frac{q\Delta t}{2m\gamma_E\Gamma}|\boldsymbol{B}|\right)$$
$$\approx 2\beta_U\frac{\gamma_B}{\gamma_E}\left(\frac{q\Delta t}{2m\Gamma}|\boldsymbol{B}|\right)^2\left\{1+\frac{1}{3}\left(\frac{q\Delta t}{2m\gamma_E\Gamma}|\boldsymbol{B}|\right)^2+\frac{2}{15}\left(\frac{q\Delta t}{2m\gamma_E\Gamma}|\boldsymbol{B}|\right)^4+\cdots\right\}^2, \tag{14e}$$

$$f_4 = \frac{q\Delta t}{m}-\frac{\gamma^{t-\frac{\Delta t}{2}}\gamma_E}{|\boldsymbol{B}|}\sin\left(\frac{q\Delta t}{m\gamma_E\Gamma}|\boldsymbol{B}|\right) = \frac{q\Delta t}{m}-2\beta_U\frac{\gamma^{t-\frac{\Delta t}{2}}\gamma_E}{|\boldsymbol{B}|}\tan\left(\frac{q\Delta t}{2m\gamma_E\Gamma}|\boldsymbol{B}|\right)$$
$$\approx \frac{q\Delta t}{m}\left[1-\beta_U\frac{\gamma^{t-\frac{\Delta t}{2}}}{\Gamma}\left\{1+\frac{1}{3}\left(\frac{q\Delta t}{2m\gamma_E\Gamma}|\boldsymbol{B}|\right)^2+\frac{2}{15}\left(\frac{q\Delta t}{2m\gamma_E\Gamma}|\boldsymbol{B}|\right)^4+\cdots\right\}\right], \tag{14f}$$

$$\beta_U = \frac{1}{1+\tan^2\left(\frac{q\Delta t}{2m\gamma_E\Gamma}|\boldsymbol{B}|\right)}$$
$$\approx \frac{1}{1+\left(\frac{q\Delta t}{2m\gamma_E\Gamma}|\boldsymbol{B}|\right)^2\left\{1+\frac{1}{3}\left(\frac{q\Delta t}{2m\gamma_E\Gamma}|\boldsymbol{B}|\right)^2+\frac{2}{15}\left(\frac{q\Delta t}{2m\gamma_E\Gamma}|\boldsymbol{B}|\right)^4+\cdots\right\}^2}. \tag{14g}$$

Here, an operator $\mathcal{F}$ with arguments of $1/\Gamma$ and Δt is defined for simplicity. The operator $\mathcal{F}$ has three forms as described below.

Taylor series expansion: If $\gamma_E^2 > 1$, i.e., $|\boldsymbol{v}_E| < c$, the numerical error of the Taylor series expansion from the tangent function becomes larger as the argument $\frac{q\Delta t}{2m\gamma_E\Gamma}|\boldsymbol{B}|$ approaches to $\pi/2$, which appears as a numerical error in the gyration angle. The operator $\mathcal{F}$ with the Taylor series expansion has an upper-bound in the numerical gyration angle per time step, $\frac{q}{m\gamma_E\Gamma}|\boldsymbol{B}|\Delta t < \pi$. If $\gamma_E^2 = \infty$, i.e., $|\boldsymbol{v}_E| = c$, γ_E disappears from the numerator of the operator $\mathcal{F}$ with the Taylor series expansion. Hence, the operator $\mathcal{F}$ is computationally stable. If $\gamma_E^2 < 0$, i.e., $|\boldsymbol{v}_E| > c$; however, the operator $\mathcal{F}$ with the Taylor series expansion becomes unstable numerically for $\beta_U < 0$, i.e., $\left(\frac{q\Delta t}{2m\gamma_E\Gamma}|\boldsymbol{B}|\right)^2 \le -1$ (Umeda 2023). Although higher-order terms of the Taylor series relax the numerically unstable condition, a safety factor given in the previous study (Umeda 2023) is necessary to avoid the numerical instability.

Tangent function: If $\gamma_E^2 > 1$, i.e., $|\boldsymbol{v}_E| < c$, the tangent function leads to overflow or underflow at $\frac{q\Delta t}{2m\gamma_E\Gamma}|\boldsymbol{B}| = \pi/2$ with some compilers. It is recommended to use cosine and sine functions instead. If $\gamma_E^2 = \infty$, i.e., $|\boldsymbol{v}_E| = c$, $\gamma_E\tan\left(\frac{q\Delta t}{2m\gamma_E\Gamma}|\boldsymbol{B}|\right)$ in Eq.(14) is replaced with $\frac{q\Delta t}{2m\Gamma}|\boldsymbol{B}|$. If $\gamma_E^2 < 0$, i.e., $|\boldsymbol{v}_E| > c$, $\tan\theta$ in Eq.(14) is replaced with $-\iota\tanh(\iota\theta)$, where ι is the imaginary unit. The operator $\mathcal{F}$ with the hyperbolic tangent function is computationally stable, since $\tanh^2(\iota\theta) < 1$.

Cosine and sine functions: If $\gamma_E^2 > 1$, i.e., $|\boldsymbol{v}_E| < c$, the cosine and sine functions do not lead to overflow or underflow for any argument. If $\gamma_E^2 = \infty$, i.e., $|\boldsymbol{v}_E| = c$, $\gamma_E\sin\left(\frac{q\Delta t}{m\gamma_E\Gamma}|\boldsymbol{B}|\right)$ and $\gamma_E^2\left\{1-\cos\left(\frac{q\Delta t}{m\gamma_E\Gamma}|\boldsymbol{B}|\right)\right\}$ in Eq.(14) is replaced with $\frac{q\Delta t}{m\Gamma}|\boldsymbol{B}|$ and $2\left(\frac{q\Delta t}{2m\Gamma}|\boldsymbol{B}|\right)^2$, respectively. That is, $f_1 = \frac{q\Delta t}{m\Gamma}$, $f_2 = f_3 = 0$, and $f_4 = \frac{q\Delta t}{m}\left(1-\gamma^{t+\frac{\Delta t}{2}}/\Gamma\right)$. If $\gamma_E^2 < 0$, i.e., $|\boldsymbol{v}_E| > c$, $\sin\theta$ and $\cos\theta$ in Eq.(14) is replaced with $-\iota\sinh(\iota\theta)$ and $\cosh(\iota\theta)$, respectively. The operator $\mathcal{F}$ with the hyperbolic cosine and sine functions is computationally stable as well.

Multi-stepping with Runge–Kutta methods

To evaluate Γ in Eq.(14) more accurately, the time integration of γ in Eq.(11) is performed with multi-step (or multi-stage) numerical integrators based on the Runge–Kutta methods (Runge 1895; Kutta 1901; Butcher 1996). This subsection provides the numerical integration with the classic fourth-order Runge–Kutta (RK4) method. The multi-step numerical integrations with other methods, i.e., Euler integrator, mid-point rule, trapezoidal rule, Heun3 integrator (Heun 1900), RK3 integrator (Kutta 1901), and Kutta-3/8 rule (Kutta 1901), are provided in Appendix A.

RK4 integrator is widely used in scientific computing in various fields, which has the fourth-order accuracy in time (Kutta 1901). The momentum vector at time $t_1 \approx t$ is estimated with the Euler integrator at the first step. The momentum vector at time $t_2 \approx t$ is re-estimated with the mid-point rule at the second step. The momentum vector at time $t_3 \approx t + \Delta t/2$ is estimated with the mid-point rule at the third step. Then, the time integration is performed based on the Simpson integration rule by using $1/\gamma^{t-\frac{\Delta t}{2}}$, $1/\gamma^{t_1}$ and $1/\gamma^{t_2}$ (at time t), and $1/\gamma^{t_3}$ (at time $t + \Delta t/2$). Finally, the momentum vector at time $t + \Delta t/2$ is obtained at the fourth step as follows:

$$\boldsymbol{u}^{t_1} = \boldsymbol{u}^{t-\frac{\Delta t}{2}} + \mathcal{F}\left(\frac{c}{\sqrt{c^2+\left|\boldsymbol{u}^{t-\frac{\Delta t}{2}}\right|^2}}, \frac{\Delta t}{2}\right), \tag{15a}$$

$$\boldsymbol{u}^{t_2} = \boldsymbol{u}^{t-\frac{\Delta t}{2}} + \mathcal{F}\left(\frac{c}{\sqrt{c^2+\left|\boldsymbol{u}^{t_1}\right|^2}}, \frac{\Delta t}{2}\right), \tag{15b}$$

$$\boldsymbol{u}^{t_3} = \boldsymbol{u}^{t-\frac{\Delta t}{2}} + \mathcal{F}\left(\frac{c}{\sqrt{c^2+\left|\boldsymbol{u}^{t_2}\right|^2}}, \Delta t\right), \tag{15c}$$

Table 1 Order of accuracy for various combinations of Taylor series terms and multi-stage integrators

Integrator	Taylor series terms			
	Δt	Δt^3	Δt^5	tan
Euler	1st	1st	1st	1st
Mid-point	2nd	2nd	2nd	2nd
Trapezoid	2nd	2nd	2nd	2nd
Heun3	2nd	3rd	3rd	3rd
RK3	2nd	3rd	3rd	3rd
RK4	2nd	4th	4th	4th
Kutta-3/8	2nd	4th	4th	4th

$$\boldsymbol{u}^{t+\frac{\Delta t}{2}} = \boldsymbol{u}^{t-\frac{\Delta t}{2}} + \mathcal{F}\left(\frac{c}{6\sqrt{c^2+\left|\boldsymbol{u}^{t_3}\right|^2}} + \frac{c}{3\sqrt{c^2+\left|\boldsymbol{u}^{t_2}\right|^2}} + \frac{c}{3\sqrt{c^2+\left|\boldsymbol{u}^{t_1}\right|^2}} + \frac{c}{6\sqrt{c^2+\left|\boldsymbol{u}^{t-\frac{\Delta t}{2}}\right|^2}}, \Delta t\right), \tag{15d}$$

$$\boldsymbol{r}^{t+\frac{\Delta t}{2}} = \boldsymbol{r}^{t-\frac{\Delta t}{2}} + \frac{\Delta t}{6}\left(\frac{c\boldsymbol{u}^{t_3}}{\sqrt{c^2+\left|\boldsymbol{u}^{t_3}\right|^2}} + \frac{2c\boldsymbol{u}^{t_2}}{\sqrt{c^2+\left|\boldsymbol{u}^{t_2}\right|^2}} + \frac{2c\boldsymbol{u}^{t_1}}{\sqrt{c^2+\left|\boldsymbol{u}^{t_1}\right|^2}} + \frac{c\boldsymbol{u}^{t-\frac{\Delta t}{2}}}{\sqrt{c^2+\left|\boldsymbol{u}^{t-\frac{\Delta t}{2}}\right|^2}}\right). \tag{15e}$$

Numerical tests

Numerical errors of the present integrators from the theoretical solution to the relativistic $E \times B$ drift in a uniform and constant electromagnetic field (Friedman and Semon 2005; Umeda 2023) are examined. For evaluating the relativistic gyration angle, the Δt term only, up to Δt^3 terms, up to Δt^5 terms of the Taylor series, and the tangent function are used. For the integration of $1/\Gamma$, Euler,

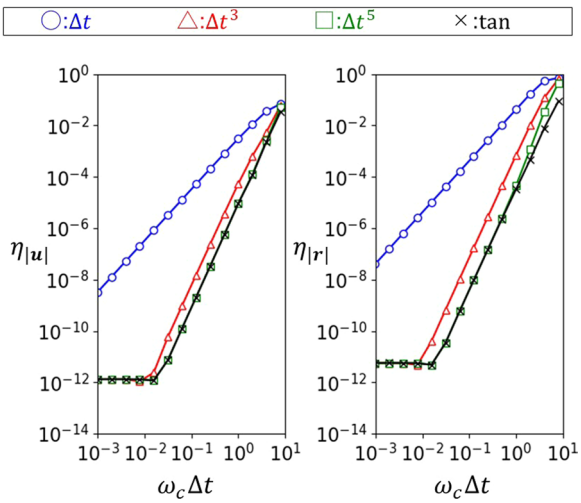

Fig. 1 Relative error η of the momentum vector $\boldsymbol{u} = (u_x, u_y)$ and position vector $\boldsymbol{r} = (x, y)$ from the theoretical solution as a function of Δt for the present integrators with the combination of RK4 and different number of Taylor series terms. The circle, triangle, square, and x-mark show the results with Δt term only, up to Δt^3 terms, up to Δt^5 terms, and tangent function, respectively

mid-point, trapezoidal, Heun3, RK3, RK4, and Kutta-3/8 integrators are used.

The order of accuracy for various combinations of the Taylor series terms and the multi-stage integrators is summarized in Table 1. The Δt term, up to Δt^3 terms, and up to Δt^5 terms of the Taylor series have the second-, fourth-, and sixth-order accuracy in time. However, the Euler integrator, i.e., $1/\Gamma = 1/\gamma^{t-\frac{\Delta t}{2}}$ has the first-order accuracy in time independently of the number of the Taylor series terms. Note that the previous Umeda integrator with the Δt term only and $1/\Gamma = 1/\gamma_-$ has the second-order accuracy in time (Umeda 2023), the choice of which is not so bad. Both of the mid-point rule and the trapezoidal rule have the second-order accuracy in time independently of the number of the Taylor series terms. The accuracy of the trapezoidal rule is slightly higher than that of the mid-point rule (not shown). The Heun3 and RK3 integrators have the third-order accuracy in time with the Taylor series terms higher than Δt but have the second-order accuracy in time with the Δt term only. The accuracy of Heun3 is almost the same as that of RK3 (not shown). The RK4 integrator and the Kutta-3/8 rule have the fourth-order accuracy in time with the Taylor series terms higher than Δt but have the second-order accuracy in time with Δt term only. The accuracy of the Kutta-3/8 rule is almost the same as that of RK4 (not shown). These results suggest that the order of accuracy is determined by the lowest order of accuracy of either the Taylor series terms or the multi-stage integrators.

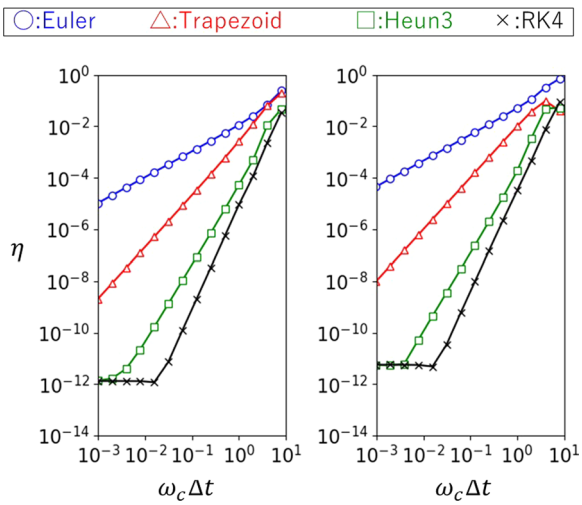

Fig. 2 Relative error η of the momentum vector $\boldsymbol{u} = (u_x, u_y)$ and position vector $\boldsymbol{r} = (x, y)$ from the theoretical solution as a function of Δt for the present integrators with the combination of the tangent function and different integrators. The circle, triangle, square, and x-mark show the results with Euler, trapezoidal, Heun3, and RK4 integrators, respectively

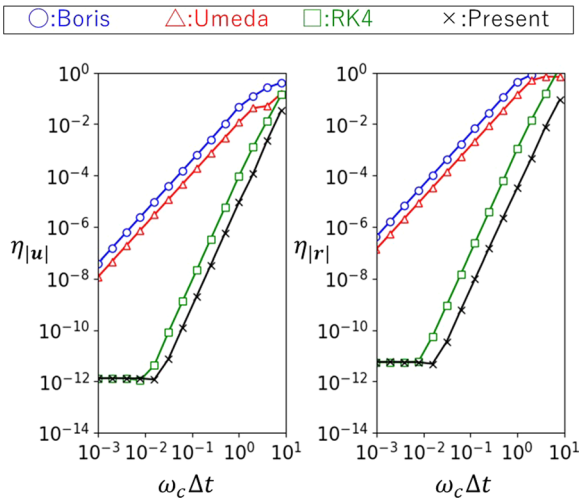

Fig. 3 Relative error η of the momentum vector $\boldsymbol{u} = (u_x, u_y)$ and position vector $\boldsymbol{r} = (x, y)$ from the theoretical solution as a function of Δt for the previous and present integrators. The circle, triangle, square, and x-mark show the results with Boris (1970), Umeda (2023), fourth-order Runge–Kutta integrators (RK4 to Eq. (1) directly), and the present study with the combination of RK4 and the tangent function, respectively

Numerical tests are performed with a uniform, constant and time-independent electromagnetic field $\boldsymbol{E} = (0, E_y, 0)$ and $\boldsymbol{B} = (0, 0, B_z)$. The $E \times B$ drift velocity $v_E = E_y/B_z = 0.8c$ and the initial velocity vector $\boldsymbol{v}_0 = (0.5c, 0, 0)$ are used. The time step is varied from $\omega_c\Delta t = 2^3$ to 2^{-9}, where $\omega_c = qB_z/m$ is the non-relativistic gyro frequency, The numerical results at $\omega_c t = 24$ is compared against the theoretical solution.

Figure 1 shows the relative error η of the momentum vector $\boldsymbol{u} = (u_x, u_y)$ and position vector $\boldsymbol{r} = (x, y)$ from the theoretical solution as a function of Δt with the combination of RK4 and different number of Taylor series terms. The circle, triangle, square, and x-mark show the results with Δt term only, up to Δt^3 terms, up to Δt^5 terms, and tangent function, respectively. It is clearly shown that the order of accuracy is second in time with Δt term only. The order of accuracy is fourth in time with more than Δt^3 terms. As the number of Taylor series terms increases, the numerical accuracy approaches to that with the tangent function. The numerical error with the Taylor series expansion is enhanced for an extremely large time step, $\frac{\omega_c\Delta t}{\gamma_E\Gamma} \geq \pi$, because of a large numerical error in the gyration angle. In Fig. 1, the maximum argument is $\omega_c\Delta t = 8$ with $\gamma_E = 5/3$ and $1.15 < \Gamma < 2.7$. The computational cost is also measured on a single compute core of the Intel Xeon Gold 6342 processor with the Intel oneAPI compiler ver.2021.5.0. The compile options are "-ipo -ip -O3 -xICELAKE-SERVER." The elapsed time per particle and per time step with Δt term only, up to

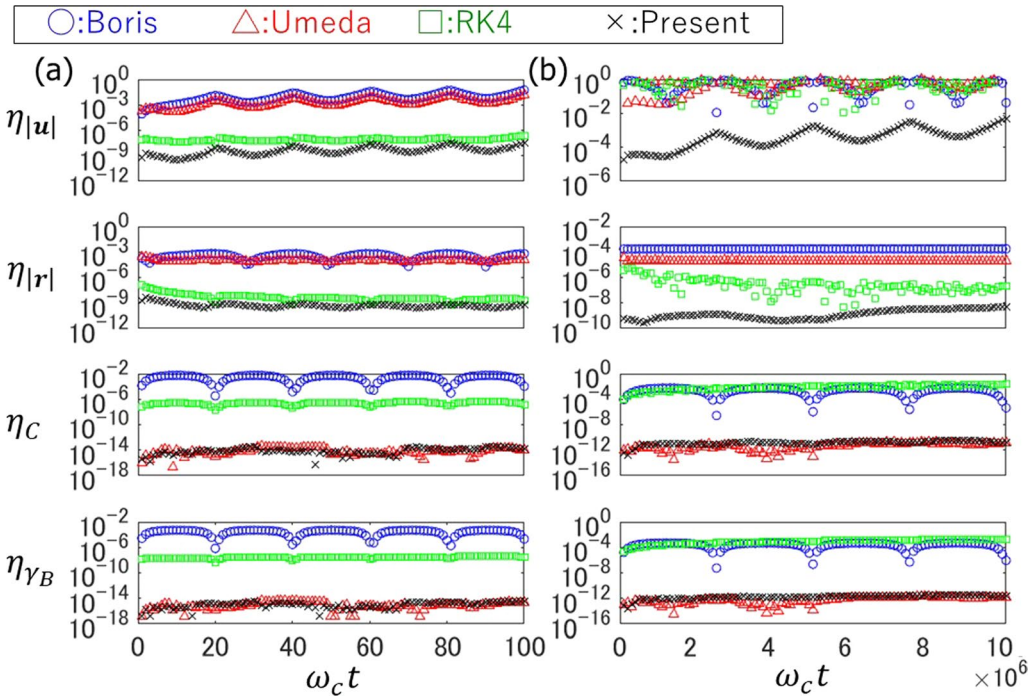

Fig. 4 Relative error η of the momentum vector $\boldsymbol{u} = (u_x, u_y)$, the position vector $\boldsymbol{r} = (x, y)$, the constant for the elliptical trajectory C in Eq. (5), and the boosted Lorentz factor γ_B in Eq.(6) from the theoretical solution as a function of time for the previous and present integrators. (a) $0 \le \omega_c t \le 100$ and (b) $0 \le \omega_c t \le 10^7$. The circle, triangle, square, and x-mark show the results with Boris (1970), Umeda (2023), fourth-order Runge–Kutta integrators (RK4 to Eq.(1) directly), and the present study with the combination of RK4 and the tangent function, respectively

Δt^3 terms, up to Δt^5 terms, and tangent function is 67.7 ns, 73.3 ns, 76.2 ns, and 94.2 ns, respectively.

Figure 2 shows relative error η of the momentum vector $\boldsymbol{u} = (u_x, u_y)$ and position vector $\boldsymbol{r} = (x, y)$ from the theoretical solution as a function of Δt with the combination of the tangent function and different integrators. The circle, triangle, square, and x-mark show the results with Euler, trapezoidal, Heun3, and RK4 integrators, respectively. It is clearly shown that the order of accuracy is first, second, third, and fourth in time with Euler, trapezoidal, Heun3, and RK4 integrators, respectively.

Figure 3 shows the relative error η of the momentum vector $\boldsymbol{u} = (u_x, u_y)$ and position vector $\boldsymbol{r} = (x, y)$ from the theoretical solution as a function of Δt for the previous and present integrators. The circle, triangle, square, and x-mark show the results with Boris (1970), Umeda (2023), fourth-order Runge–Kutta integrators (RK4 to Eq.(1) directly), and the present study with the combination of RK4 and the tangent function, respectively. It is shown that the numerical error of direct RK4 is much lower than that of both Boris (1970) and Umeda (2023) integrators. The numerical error of the present study is two orders lower than that of direct RK4. The elapsed time per particle and per time step with the Umeda integrator is 58.4 ns. Hence, the numerical cost of the present study is much cheaper than that of the previous study.

A long-term numerical test is also performed with the same electromagnetic field $\boldsymbol{E} = (0, E_y, 0)$ and $\boldsymbol{B} = (0, 0, B_z)$, the $E \times B$ drift velocity $v_E = E_y/B_z = 0.8c$, and the initial velocity vector $\boldsymbol{v}_0 = (0.5c, 0, 0)$. The time step is fixed to $\omega_c \Delta t = 0.1$, and the numerical test is performed up to $\omega_c t = 10^7$. Figure 4 shows the relative error η of the momentum vector $\boldsymbol{u} = (u_x, u_y)$, the position vector $\boldsymbol{r} = (x, y)$, the constant for the elliptical trajectory C in Eq.(5), and the boosted Lorentz factor γ_B in Eq.(6) from the theoretical solution as a function of time for the previous and present integrators.

For a short-term numerical test, the numerical errors in the momentum and position vectors with the second-order (Boris and Umeda), RK4, and present integrators are $\sim 10^{-4}$, $\sim 10^{-8}$, and $\sim 10^{-10}$, respectively, which is consistent with Fig. 3. The numerical error in the constant for the elliptical trajectory C with the Boris integrator varies between 10^{-6} and 10^{-2} at a certain period ($T \approx 20/\omega_c$ in the present case), which depends on γ_E and γ_B. This result indicates that the momentum vector moves along an elliptical trajectory with a wrong relativistic $E \times B$ drift velocity. The numerical error in the

boosted Lorentz factor γ_B is related to the numerical error in C, because the center of the elliptical trajectory is given as $(\gamma_B\gamma_E v_E, 0)$. The numerical error in the constant for the elliptical trajectory C with RK4 is $\sim 10^{-8}$. On the other hand, the numerical errors in the constant for the elliptical trajectory C with the Umeda and present integrators are $\sim 10^{-14}$.

For a long-term numerical test, the numerical errors in the momentum vectors with the Boris and Umeda integrators vary between 10^{-2} and 10^{0} because of the accumulation of the numerical error in the gyration angle. The numerical error in the momentum vectors with the present integrator is much lower than that with other integrators. Note that oscillations in the numerical errors in Fig. 4b are due to a data sampling rate. The numerical errors in the position vector with the Boris, Umeda, and present integrators are $\sim 10^{-4}$, $\sim 10^{-5}$ and $\sim 10^{-8}$, respectively. The numerical error in the constant for the elliptical trajectory C with RK4 increases to 10^{-2}, which indicates that the momentum vector deviates from the theoretical trajectory. On the other hand, the numerical error in C with the Boris integrator varies between 10^{-6} and 10^{-2}, which indicates that the momentum vector is on the elliptical trajectory for a long term. The numerical errors in C and γ_B with the Umeda and present integrators are $\sim 10^{-12}$. The result clearly shows that the operator $\mathcal{F}$ in Eq.(14) is well-designed for conserving both C and γ_B.

It is noted that the operator $\mathcal{F}(1/\Gamma, \Delta t)$ is Eq.(14) is replaced with $\mathcal{F}[1/\Gamma, \boldsymbol{E}^t(\boldsymbol{r}^t), \boldsymbol{B}^t(\boldsymbol{r}^t), \Delta t]$ with the position vector obtained with the multi-stage numerical integrator, if electromagnetic fields are non-uniform and time-dependent.

Conclusions

Instead of the classic Runge–Kutta (RK4) integrator (Runge 1895; Kutta 1901), the relativistic equations of motion for charged particles have been conventionally solved with the Boris integrator (or the Boris push) (Boris 1970) in particle-in-cell (PIC) plasma simulations. The conventional Boris integrator (Boris 1970), the previous Vay (2008) and Higuera and Cary (2017) integrators conserve the kinetic energy of charged particles during the gyration but have large numerical errors in the relativistic $E \times B$ drift velocity. Recently, a new integrator (the Umeda integrator) has been developed, which provides the exact relativistic $E \times B$ drift velocity (Umeda 2023). However, the Umeda integrator has the second-order accuracy in time and has a numerical error in the relativistic gyration angle as well.

To reduce the numerical error of the Umeda integrator and to make its order of accuracy higher, two advanced numerical techniques are adopted in the present study. One is the Taylor series expansion of the numerical gyration angle (Kato and Zenitani 2021), and the other is multi-step (multi-stage) Runge–Kutta method (Butcher 1996) for the integration of the Lorentz factor. With the combination of the trigonometric function for the gyration angle and RK4 for the integration of the Lorentz factor, a new fourth-order integrator has been developed. The new integrator conserves both of the kinetic energy of charged particles during the gyration and the relativistic boosted Lorentz factor, but has a numerical accuracy much higher than the classic RK4. The computational cost of the new integrator is much cheaper than the Umeda integrator. Although the order of accuracy is extended up to fourth in the present study, higher-order multi-stage integrators for the integration of the Lorentz factor could make the order of accuracy higher in time.

Appendix A: Multi-stepping with other Runge–Kutta methods

Euler integrator

The Euler integrator is known as an explicit time-forwarding numerical procedure with the first-order accuracy in time. The momentum vector is updated with $1/\Gamma = 1/\gamma^{t-\frac{\Delta t}{2}}$ as follows:

$$\boldsymbol{u}^{t+\frac{\Delta t}{2}} = \boldsymbol{u}^{t-\frac{\Delta t}{2}} + \mathcal{F}\left(\frac{c}{\sqrt{c^2 + \left|\boldsymbol{u}^{t-\frac{\Delta t}{2}}\right|^2}}, \Delta t\right), \tag{A.1a}$$

$$\boldsymbol{r}^{t+\frac{\Delta t}{2}} = \boldsymbol{r}^{t-\frac{\Delta t}{2}} + \Delta t \frac{c\boldsymbol{u}^{t-\frac{\Delta t}{2}}}{\sqrt{c^2 + \left|\boldsymbol{u}^{t-\frac{\Delta t}{2}}\right|^2}}. \tag{A.1b}$$

Mid-point rule

The numerical integrator based on the mid-point rule has second-order accuracy in time. The momentum vector at time t is estimated with the Euler integrator at the first step. Then, by assuming that $1/\Gamma = 1/\gamma^t$ is constant in time from $t - \Delta t/2$ to $t + \Delta t/2$, the momentum vector at time $t + \Delta t/2$ is obtained at the second step as follows:

$$\boldsymbol{u}^{t} = \boldsymbol{u}^{t-\frac{\Delta t}{2}} + \mathcal{F}\left(\frac{c}{\sqrt{c^2 + \left|\boldsymbol{u}^{t-\frac{\Delta t}{2}}\right|^2}}, \frac{\Delta t}{2}\right), \tag{A.2a}$$

$$\boldsymbol{u}^{t+\frac{\Delta t}{2}} = \boldsymbol{u}^{t-\frac{\Delta t}{2}} + \mathcal{F}\left(\frac{c}{\sqrt{c^2+\left|\boldsymbol{u}^{t}\right|^2}}, \Delta t\right), \tag{A.2b}$$

$$\boldsymbol{r}^{t+\frac{\Delta t}{2}} = \boldsymbol{r}^{t-\frac{\Delta t}{2}} + \Delta t \frac{c\boldsymbol{u}^{t}}{\sqrt{c^2+\left|\boldsymbol{u}^{t}\right|^2}}. \tag{A.2c}$$

Trapezoidal rule

The numerical integrator based on the trapezoidal rule has second-order accuracy in time. The momentum vector at time $t_1 \approx t + \Delta t/2$ is estimated with the Euler integrator at the first step. By assuming that $1/\gamma$ changes linearly from $1/\gamma^{t-\Delta t/2}$ to $1/\gamma^{t_1}$, $1/\Gamma$ is obtained with the numerical integration based on the trapezoidal rule. Then, the momentum vector at time $t + \Delta t/2$ is obtained at the second step as follows:

$$\boldsymbol{u}^{t_1} = \boldsymbol{u}^{t-\frac{\Delta t}{2}} + \mathcal{F}\left(\frac{c}{\sqrt{c^2+\left|\boldsymbol{u}^{t-\frac{\Delta t}{2}}\right|^2}}, \Delta t\right), \tag{A.3a}$$

$$\boldsymbol{u}^{t+\frac{\Delta t}{2}} = \boldsymbol{u}^{t-\frac{\Delta t}{2}} + \mathcal{F}\left(\frac{c}{2\sqrt{c^2+\left|\boldsymbol{u}^{t_1}\right|^2}} + \frac{c}{2\sqrt{c^2+\left|\boldsymbol{u}^{t-\frac{\Delta t}{2}}\right|^2}}, \Delta t\right), \tag{A.3b}$$

$$\boldsymbol{r}^{t+\frac{\Delta t}{2}} = \boldsymbol{r}^{t-\frac{\Delta t}{2}} + \frac{\Delta t}{2}\left(\frac{c\boldsymbol{u}^{t_1}}{\sqrt{c^2+\left|\boldsymbol{u}^{t_1}\right|^2}} + \frac{c\boldsymbol{u}^{t-\frac{\Delta t}{2}}}{\sqrt{c^2+\left|\boldsymbol{u}^{t-\frac{\Delta t}{2}}\right|^2}}\right). \tag{A.3c}$$

Heun3 integrator

The third-order Heun (Heun3) integrator is known as an explicit time-forwarding numerical procedure with the third-order accuracy in time (Heun 1900). The momentum vector at time $t - \Delta t/6$ is estimated with the Euler integrator at the first step. Then, the momentum vector at time $t + \Delta t/6$ is estimated with the mid-point rule at the second step. Finally, the momentum vector at time $t + \Delta t/2$ is obtained at the third step as follows:

$$\boldsymbol{u}^{t-\frac{\Delta t}{6}} = \boldsymbol{u}^{t-\frac{\Delta t}{2}} + \mathcal{F}\left(\frac{c}{\sqrt{c^2+\left|\boldsymbol{u}^{t-\frac{\Delta t}{2}}\right|^2}}, \frac{\Delta t}{3}\right), \tag{A.4a}$$

$$\boldsymbol{u}^{t+\frac{\Delta t}{6}} = \boldsymbol{u}^{t-\frac{\Delta t}{2}} + \mathcal{F}\left(\frac{c}{\sqrt{c^2+\left|\boldsymbol{u}^{t-\frac{\Delta t}{6}}\right|^2}}, \frac{2\Delta t}{3}\right), \tag{A.4b}$$

$$\boldsymbol{u}^{t+\frac{\Delta t}{2}} = \boldsymbol{u}^{t-\frac{\Delta t}{2}} + \mathcal{F}\left(\frac{3c}{4\sqrt{c^2+\left|\boldsymbol{u}^{t+\frac{\Delta t}{6}}\right|^2}} + \frac{c}{4\sqrt{c^2+\left|\boldsymbol{u}^{t-\frac{\Delta t}{2}}\right|^2}}, \Delta t\right), \tag{A.4c}$$

$$\boldsymbol{r}^{t+\frac{\Delta t}{2}} = \boldsymbol{r}^{t-\frac{\Delta t}{2}} + \frac{\Delta t}{4}\left(\frac{3c\boldsymbol{u}^{t+\frac{\Delta t}{6}}}{\sqrt{c^2+\left|\boldsymbol{u}^{t+\frac{\Delta t}{6}}\right|^2}} + \frac{c\boldsymbol{u}^{t-\frac{\Delta t}{2}}}{\sqrt{c^2+\left|\boldsymbol{u}^{t-\frac{\Delta t}{2}}\right|^2}}\right). \tag{A.4d}$$

RK3 integrator

The third-order Runge–Kutta (RK3) integrator is known as an explicit numerical procedure with the third-order accuracy in time (Kutta 1901). The momentum vector at time t is estimated with the Euler integrator at the first step. The momentum vector at time $t_1 \approx t + \Delta t/2$ is estimated at the second step. By assuming that $1/\gamma$ changes in a parabolic manner from $1/\gamma^{t-\Delta t/2}$ to $1/\gamma^{t_1}$ via $1/\gamma^{t}$, $1/\Gamma$ is obtained with the numerical integration based on the Simpson integration rule. Finally, the momentum vector at time $t + \Delta t/2$ is obtained at the third step as follows:

$$\boldsymbol{u}^{t} = \boldsymbol{u}^{t-\frac{\Delta t}{2}} + \mathcal{F}\left(\frac{c}{\sqrt{c^2+\left|\boldsymbol{u}^{t-\frac{\Delta t}{2}}\right|^2}}, \frac{\Delta t}{2}\right), \tag{A.5a}$$

$$\boldsymbol{u}^{t_1} = \boldsymbol{u}^{t-\frac{\Delta t}{2}} + \mathcal{F}\left(\frac{2c}{\sqrt{c^2+\left|\boldsymbol{u}^{t}\right|^2}} - \frac{c}{\sqrt{c^2+\left|\boldsymbol{u}^{t-\frac{\Delta t}{2}}\right|^2}}, \Delta t\right), \tag{A.5b}$$

$$\boldsymbol{u}^{t+\frac{\Delta t}{2}} = \boldsymbol{u}^{t-\frac{\Delta t}{2}} + \mathcal{F}\left(\frac{c}{6\sqrt{c^2+\left|\boldsymbol{u}^{t_1}\right|^2}} + \frac{2c}{3\sqrt{c^2+\left|\boldsymbol{u}^{t}\right|^2}} + \frac{c}{6\sqrt{c^2+\left|\boldsymbol{u}^{t-\frac{\Delta t}{2}}\right|^2}}, \Delta t \right), \tag{A.5c}$$

$$\boldsymbol{r}^{t+\frac{\Delta t}{2}} = \boldsymbol{r}^{t-\frac{\Delta t}{2}} + \frac{\Delta t}{6}\left(\frac{c\boldsymbol{u}^{t_1}}{\sqrt{c^2+\left|\boldsymbol{u}^{t_1}\right|^2}} + \frac{4c\boldsymbol{u}^{t}}{\sqrt{c^2+\left|\boldsymbol{u}^{t}\right|^2}} + \frac{c\boldsymbol{u}^{t-\frac{\Delta t}{2}}}{\sqrt{c^2+\left|\boldsymbol{u}^{t-\frac{\Delta t}{2}}\right|^2}} \right). \tag{A.5d}$$

Kutta-3/8 rule

There is another version of the fourth-order Runge–Kutta integrator, which is known as the Kutta-3/8 rule (Kutta 1901). The momentum vector at time $t-\frac{\Delta t}{6}$ is estimated with the Euler integrator at the first step. The momentum vector at time $t+\frac{\Delta t}{6}$ is estimated at the second step. The momentum vector at time $t_1 \approx t+\Delta t/2$ is estimated at the third step. Then, the time integration is performed based on the numerical integration of a cubic polynomial function passing through four points of $1/\gamma^{t-\frac{\Delta t}{2}}$, $1/\gamma^{t-\frac{\Delta t}{6}}$, $1/\gamma^{t+\frac{\Delta t}{6}}$, and $1/\gamma^{t_1}$ (at time $t+\Delta t/2$). Finally, the momentum vector at time $t+\Delta t/2$ is obtained at the fourth step as follows:

$$\boldsymbol{u}^{t-\frac{\Delta t}{6}} = \boldsymbol{u}^{t-\frac{\Delta t}{2}} + \mathcal{F}\left(\frac{c}{\sqrt{c^2+\left|\boldsymbol{u}^{t-\frac{\Delta t}{2}}\right|^2}}, \frac{\Delta t}{3} \right), \tag{A.6a}$$

$$\boldsymbol{u}^{t+\frac{\Delta t}{6}} = \boldsymbol{u}^{t-\frac{\Delta t}{2}} + \mathcal{F}\left(\frac{c}{\sqrt{c^2+\left|\boldsymbol{u}^{t-\frac{\Delta t}{2}}\right|^2}} - \frac{c}{3\sqrt{c^2+\left|\boldsymbol{u}^{t-\frac{\Delta t}{2}}\right|^2}}, \frac{2\Delta t}{3} \right), \tag{A.6b}$$

$$\boldsymbol{u}^{t_1} = \boldsymbol{u}^{t-\frac{\Delta t}{2}} + \mathcal{F}\left(\frac{c}{\sqrt{c^2+\left|\boldsymbol{u}^{t+\frac{\Delta t}{6}}\right|^2}} - \frac{c}{\sqrt{c^2+\left|\boldsymbol{u}^{t-\frac{\Delta t}{6}}\right|^2}} + \frac{c}{\sqrt{c^2+\left|\boldsymbol{u}^{t-\frac{\Delta t}{2}}\right|^2}}, \Delta t \right), \tag{A.6c}$$

$$\boldsymbol{u}^{t+\frac{\Delta t}{2}} = \boldsymbol{u}^{t-\frac{\Delta t}{2}} + \mathcal{F}\left(\frac{c}{8\sqrt{c^2+\left|\boldsymbol{u}^{t_1}\right|^2}} + \frac{3c}{8\sqrt{c^2+\left|\boldsymbol{u}^{t+\frac{\Delta t}{6}}\right|^2}} + \frac{3c}{8\sqrt{c^2+\left|\boldsymbol{u}^{t-\frac{\Delta t}{6}}\right|^2}} + \frac{c}{8\sqrt{c^2+\left|\boldsymbol{u}^{t-\frac{\Delta t}{2}}\right|^2}}, \Delta t \right), \tag{A.6d}$$

$$\boldsymbol{r}^{t+\frac{\Delta t}{2}} = \boldsymbol{r}^{t-\frac{\Delta t}{2}} + \frac{\Delta t}{8}\left(\frac{c\boldsymbol{u}^{t_1}}{\sqrt{c^2+\left|\boldsymbol{u}^{t_1}\right|^2}} + \frac{3c\boldsymbol{u}^{t+\frac{\Delta t}{6}}}{\sqrt{c^2+\left|\boldsymbol{u}^{t+\frac{\Delta t}{6}}\right|^2}} + \frac{3c\boldsymbol{u}^{t-\frac{\Delta t}{6}}}{\sqrt{c^2+\left|\boldsymbol{u}^{t-\frac{\Delta t}{6}}\right|^2}} + \frac{c\boldsymbol{u}^{t-\frac{\Delta t}{2}}}{\sqrt{c^2+\left|\boldsymbol{u}^{t-\frac{\Delta t}{2}}\right|^2}} \right). \tag{A.6e}$$

Abbreviations

PIC Particle-in-cell
RK Runge–Kutta

Acknowledgements
This work was conducted as a computational joint research program at the Institute for Space-Earth Environmental Research, Nagoya University.

Author contributions
TU developed the new scheme and drafted the manuscript. RO developed the numerical codes, performed the numerical tests, and analyzed the numerical results. Both of authors read and approved the final manuscript.

Funding
This work was supported by MEXT/JSPS under Grant-In-Aid (KAKENHI) for Scientific Research (B) No. JP19H01868.

Availability of data and materials
The numerical code used in the present study is available from the corresponding author on reasonable request.

Declarations

Ethics approval and consent to participate
Not applicable.

Consent for publication
Not applicable.

Competing interests
The authors declare that they have no competing interests.

Author details
[1]Institute for Space-Earth Environmental Research, Nagoya University, Nagoya 464-8601, Japan.

Received: 29 April 2023 Accepted: 8 September 2023
Published online: 10 October 2023

References

Boris JP (1970) Relativistic plasma simulation-optimization of a hybrid code. In: Proceedings of 4th Conference on Numerical Simulation of Plasmas, Washington D.C. 3–67
Butcher JC (1996) A history of Runge-Kutta methods. Appl Num Math 20:247–260. https://doi.org/10.1016/0168-9274(95)00108-5
Friedman Y, Semon MD (2005) Relativistic acceleration of charged particles in uniform and mutually perpendicular electric and magnetic fields as viewed in the laboratory frame. Phys Rev E 72:026603. https://doi.org/10.1103/PhysRevE.72.026603
Fujiwara Y, Nogi T, Omura Y (2022) Nonlinear triggering process of whistler-mode emissions in a homogeneous magnetic field. Earth Planets Space 74:95. https://doi.org/10.1186/s40623-022-01646-x
He Y, Sun Y, Liu J, Qin H (2015) Volume-preserving algorithms for charged particle dynamics. J Comput Phys 281:135–147. https://doi.org/10.1016/j.jcp.2014.10.032
Higuera AV, Cary JR (2017) Structure-preserving second-order integration of relativistic charged particle trajectories in electromagnetic fields. Phys Plasmas 24:052104. https://doi.org/10.1063/1.4979989
Hiraga R, Omura Y (2020) Acceleration mechanism of radiation belt electrons through interaction with multi-subpacket chorus waves. Earth Planets Space 72:21. https://doi.org/10.1186/s40623-020-1134-3
Heun K (1900) Neue methoden zur approximativen Integration der differentialgleichungen eincr unabläingigen veränderliehen. Z Math Phys 45:23–38
Kato TN, Zenitani S (2021) Volume-preserving particle integrator based on exact flow of velocity for nonrelativistic particle-in-cell simulations. arXiv:2108.02426 [physics.plasm-ph].
Katoh Y (2014) A simulation study of the propagation of whistler-mode chorus in the Earth's inner magnetosphere. Earth Planet Space 66:6. https://doi.org/10.1186/1880-5981-66-6
Katoh Y, Omura Y (2016) Electron hybrid code simulation of whistler-mode chorus generation with real parameters in the Earth's inner magnetosphere. Earth Planets Space 68:192. https://doi.org/10.1186/s40623-016-0568-0
Kutta MW (1901) Beitrag zur näherungsweisen integration totaler differentialgleichungen. Z Math Phys 46:435–453
Nakanotani M, Hada T, Matsukiyo S (2018) Diffusive shock acceleration of cosmic rays from two stationary shocks. Earth Planets Space 70:33. https://doi.org/10.1186/s40623-018-0799-3
Omura Y (2021) Nonlinear wave growth theory of whistler-mode chorus and hiss emissions in the magnetosphere. Earth Planets Space 73:95. https://doi.org/10.1186/s40623-021-01380-w
Qin H, Zhang S, Liu J, Sun Y, Tang WM (2013) Why is Boris algorithm so good? Phys Plasmas 20:084503. https://doi.org/10.1063/1.4818428
Ripperda B, Bacchini F, Teunissen J, Xia C, Porth O, Sironi L, Lapenta G, Keppens R (2018) A comprehensive comparison of relativistic particle integrators. Astrophys J Suppl Ser 235:21. https://doi.org/10.3847/1538-4365/aab114
Runge C (1895) Ueber die numerische auflösung von differentialgleichungen. Math Ann 46:167–178. https://doi.org/10.1007/BF01446807
Umeda T (2023) A new integrator for relativistic E-cross-B motion of charged particles. J Comput Phys 472:111694. https://doi.org/10.1016/j.jcp.2022.111694
Umeda T, Yamazaki R (2006) Full particle simulation of a perpendicular collisionless shock: a shock-rest-frame model. Earth Planet Space 58:e41–e44. https://doi.org/10.1186/BF03352617
Vay J-L (2008) Simulation of beams or plasmas crossing at relativistic velocity. Phys Plasmas 15:056701. https://doi.org/10.1063/1.2837054
Zenitani S, Umeda T (2018) On the Boris solver in particle-in-cell simulation. Phys Plasmas 25:112110. https://doi.org/10.1063/1.5051077
Zhang R, Liu J, Qin H, Wang Y, He Y, Sun Y (2015) Volume-preserving algorithm for secular relativistic dynamics of charged particles. Phys Plasmas 22:044501. https://doi.org/10.1063/1.4916570

Publisher's Note